LA-UR- 08-7144

Approved for public release; distribution is unlimited.

Title:	"Tuning Magnetic Disorder in Diluted Magnetic Semiconductors Using High Fields to 89 Tesla"
Author(s):	Scott Crooker, MPA-NHMFL, LANL Nitin Samarth, Pennsylvania State University
Intended for:	International Journal Modern Phys. B Conference Proceedings for HMF-18 Conference on High Magnetic Fields in Semiconductor Physics Sao Pedro, Brazil August 2-9, 2008

Los Alamos
NATIONAL LABORATORY
EST. 1943

Form 836 (7/06)

International Journal of Modern Physics B

TUNING MAGNETIC DISORDER IN DILUTED MAGNETIC SEMICONDUCTORS USING HIGH FIELDS TO 89 TESLA

SCOTT A. CROOKER

National High Magnetic Field Laboratory
Mail Stop E536, Los Alamos National Laboratory
Los Alamos, New Mexico 87545, USA
crooker@lanl.gov

NITIN SAMARTH

Department of Physics, Pennsylvania State University
University Park, Pennsylvania 16802, USA

Received Day Month Year
Revised Day Month Year

We describe recent and ongoing studies at the National High Magnetic Field Laboratory at Los Alamos using the new "100 Tesla Multi-Shot Magnet", which is presently delivering fields up to ~89 T during its commissioning. We discuss the first experiments performed in this magnet system, wherein the linewidth of low-temperature photoluminescence spectra was used to directly reveal the degree of magnetic alloy disorder 'seen' by excitons in single $Zn_{0.80}Cd_{0.22}Mn_{0.08}Se$ quantum wells. The magnetic potential landscape in II-VI diluted magnetic semiconductors (DMS) is typically smoothed when the embedded Mn^{2+} spins align in an applied field. However, an important (but heretofore untested) prediction of current models of compositional disorder is that magnetic alloy fluctuations in many DMS compounds should *increase* again in very large magnetic fields approaching 100 T. We observed precisely this increase above ~70 T, in agreement with a simple model of magnetic alloy disorder.

Keywords: magnetic semiconductor; high magnetic field; alloy disorder.

1. Introduction

High magnetic fields are an important tool for many condensed-matter physics experiments. For example, high fields have been used with great success to study organic and high-T_c superconductors, correlated electron systems, heavy fermion materials and Kondo insulators, and of course semiconductor quantum structures.[1] Pulsed magnets with durations in the tens of milliseconds are typically limited to fields of order 50-70 T, while the generation of even higher magnetic fields typically requires semi-destructive or completely destructive magnets having much shorter microsecond pulse durations (such as single-turn or flux-compression techniques). Several pulsed-field laboratories around the globe are pursuing magnet technologies capable of delivering millisecond-duration fields in the megagauss range (100 T), in

a non-destructive fashion. The "100 T Multi-Shot Magnet" at the National High Magnetic Field Laboratory (NHMFL) at Los Alamos directly addresses this need and is currently being commissioned. This paper describes the magnet itself and details the first experiments performed in this magnet. These photoluminescence (PL) studies address a long-standing, but heretofore unverified, prediction in diluted magnetic semiconductor (DMS) materials – namely, that the degree of magnetic alloy disorder in certain DMS materials will be annealed (smoothed) in large fields to ~70 T, but will then increase (become *rougher*) in even larger magnetic fields. Using PL linewidths as a probe of the microscopic magnetic alloy disorder in single DMS quantum wells, we verified this prediction explicitly,[2] thereby validating a simple model of compositional disorder in these semiconductor systems.

2. The "100 Tesla Multi-Shot Magnet"

Figure 1 shows a schematic of the "100 T Multi-Shot Magnet". The magnet is currently delivering pulses to ~89 T, non-destructively, during its ongoing commissioning phase. The magnet consists of three outer coils and an inner coil. The outer coils are powered by a 1.4 GVA motor-generator that stores ~650 MJ of energy.

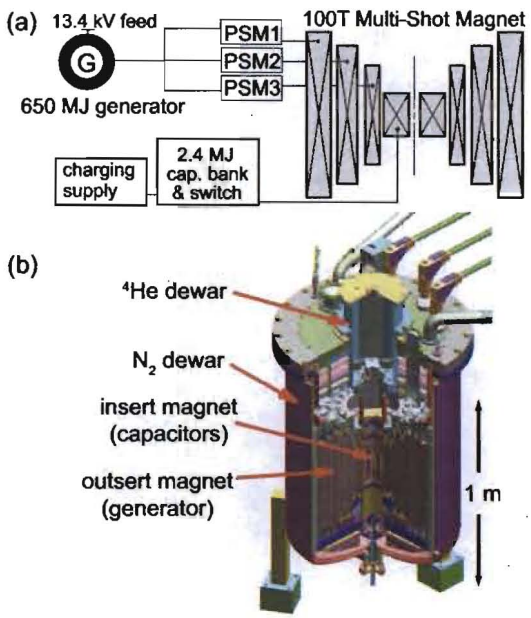

Fig. 1. a) A schematic of the 100 T Multi-Shot Magnet. The outer coil sets are powered by a 1.4 GVA motor-generator and three power supply modules (PSM), while the insert coil is driven by a 2.4 MJ capacitor bank. b) A cut-away drawing of the 100 T magnet assembly and cryostat.

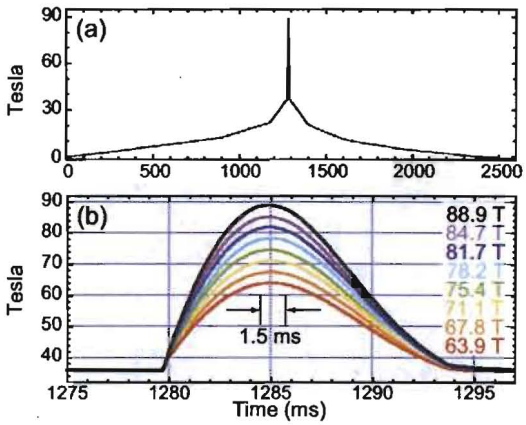

Fig. 2. a) A plot of the measured magnetic field versus time for an 88.9 T pulse. The outer coils generate the 2.5 second long 'pedestal' field, upon which the inner coil provides the short (~12 ms) pulse to peak field. b) An expanded view showing eight different high-field pulses. All pulses used the same 'pedestal' field from the outer coils, while the charging voltage on the capacitor bank that drives the inner coils was increased from 7 to 14 kV in 1 kV increments. Reproduced from Ref. (2).

In this work, the outer coils provide a 2.5 second long 'pedestal' pulse having peak field ~36 T. The insert coil is powered by a separate 18 kV, 2.4 MJ capacitor bank, providing an additional 54 T in a short pulse of ~12 ms duration. The present insert coil is rated to 90 T, and an insert coil capable of the full 100 T is scheduled for replacement in the future.

Figure 2(a) shows the measured field profile of an 88.9 T pulse. An expanded view of this (and seven other) pulses is shown in Fig. 2(b). Here, the outer coils provided the same 'pedestal', while the field generated by the insert coil was increased by charging the capacitor bank from 7 to 14 kV in 1 kV increments, giving maximum fields from 63.9 to 88.9 T. A calibrated pickup coil on the sample probe was used to measure the field, and we estimate that integration errors give ±0.5 T uncertainty.

3. Experimental techniques

To date, several different experimental techniques have been demonstrated to work extremely well in this magnet. The first is optical spectroscopy, which will be described shortly. Another method is magnetometry using balanced pickup coils, to measure quantum oscillations due to de Haas-van Alphen effects at ultrahigh magnetic fields. Here, the relatively fast and noise-free increase of the magnetic field from the insert coil gives very clean dHvA signals. This method was recently used[3] to observe the reconstruction of the Fermi surface above the 61 T Néel critical field in $CeIn_3$. A third method that has found much success is "contactless conductivity", in which samples reside in the inductor of an LC tank circuit that is

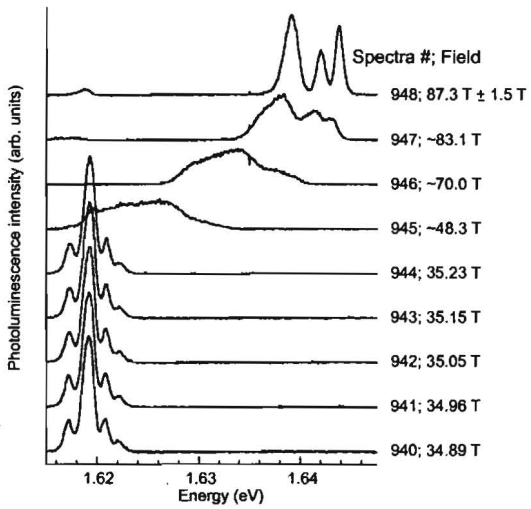

Fig. 3. This plot shows one of the first measurements performed in this magnet. The data show nine PL spectra (#940-948) that were sequentially acquired every 1.5 ms up to the peak magnetic field of ~87.3 T. The sample was a CdTe-based 2D electron gas at 1.6 K, and the multiple emission peaks are due to neutral and charged exciton complexes. The inner magnet coil fired while the sixth spectra was being acquired, leading to smearing of the PL in this and the next two spectra. However, the field varied by only ~1.5 T during acquisition of the spectra at peak field.

driven by a tunnel-diode oscillator. Changes in the sample's conductivity modify L, changing the circuit's resonant frequency which is measured with high precision throughout the field pulse. Using this method, Shubnikov-de Haas oscillations in the underdoped cuprate $YBa_2Cu_4O_8$ were measured for the first time.[4]

Because this magnet provides ultrahigh fields with relatively long (millisecond) durations, PL spectroscopy is possible. Using reasonably 'bright' samples and fast spectral acquisition rates (~1 ms/spectra), very good PL signals can be obtained. Typical PL studies use single 600 μm diameter optical fibers to carry excitation light to the sample in the bore of the magnet, and PL is collected back through the same fiber where it is dispersed in a spectrometer and detected with liquid-nitrogen cooled CCD or diode array detectors (for visible and IR light, respectively). Polarization analysis is accomplished using thin-film polarizers sandwiched between the fiber and the sample. High-resolution spectra are continuously acquired throughout the magnetic field pulse, using acquisition times as fast as 1.2 ms/spectra.

Figure 3 shows an example of PL from a single CdTe-based 2D electron gas at 1.6 K. 2000 spectra were acquired throughout this 87.3 T pulse; the Figure shows the nine spectra (#940→#948) that were acquired just prior to (and including) peak field. The first five spectra were acquired at the top of the 'pedestal' generated by the outer coils, and the field variation per spectra is small. (The multiple PL

peaks are due to neutral and charged excitons[5]). The inner coil began ramping during acquisition of the sixth spectra. The field increases rapidly during this and the next two spectra, leading to considerable smearing of the PL spectra. However, the last (ninth) spectra was acquired during peak field, where the field does not vary much (±1.5 T or so) during the 1.5 ms acquisition. It is clear, then, that accurate PL measurements as a function of field using this magnet – particularly if one is interested in variations of PL linewidth – necessitate multiple magnet pulses, wherein only the spectra acquired at peak field are usable. While this does represent a limitation, it nonetheless does allow for the first time the measurement of high-resolution PL spectra in magnetic fields exceeding ~60 T.

4. Tuning magnetic disorder in DMS quantum wells

The first complete study performed in this magnet used high-resolution PL spectroscopy to measure the degree of magnetic disorder in single DMS quantum wells.[2] The linewidth of band-edge PL is a powerful probe of disorder and crystal quality in compound semiconductors such as $Al_xGa_{1-x}As$. Compositional alloy disorder exists due to the random placement of cation (or anion) species. This intrinsic alloy disorder presents a microscopic fluctuation potential that can be directly inferred from the PL linewidth, Γ. Photoexcited excitons act as mesoscopic probes of local disorder, where each exciton averages the alloy fluctuations over the atoms within its wavefunction. The standard deviation of exciton energies gives the broadened PL linewidth. Γ can therefore be modeled by the statistics of alloy fluctuations over the N cation sites within the exciton's nominal 'volume'.

Models have been developed to quantify microscopic alloy fluctuations in compound semiconductors and to correlate this disorder with measurements of Γ. Initial work focused on non-magnetic semiconductors, in which alloy fluctuations are fixed for a given sample.[6,7,8] More recently, alloy disorder in II-VI diluted magnetic semiconductors (DMS) has been studied.[9,10,11,12] In DMS the alloy disorder potential *within a given sample* can be tuned as the magnetic spins (usually spin-$\frac{5}{2}$ Mn) align in an applied magnetic field, H. DMS therefore provide a flexible system against which to benchmark models of alloy disorder. As Fig. 4 depicts, experiments to date have shown a decrease in Γ as Mn spins align in low H, and as Mn spin clusters begin to align in high H to 60 T, in approximate agreement with models. However, a critical and as-yet-unverified aspect of current models is the expectation that alloy disorder in many DMS materials should *increase* again as antiferromagnetically-bound clusters of Mn spins achieve full alignment at very high magnetic fields.[10] This field scale is typically quite large, of order 50-100 T.

We therefore measure Γ from a single $Zn_{.70}Cd_{.22}Mn_{.08}Se$ quantum well to ~89 T. Above 70 T, we observe that Γ markedly increases, in qualitative agreement with a simple 'local-bandgap' model of compositional alloy disorder. These data further validate current models of field-tunable alloy disorder in DMS materials, and support 'local-bandgap' approaches to alloy disorder in general.

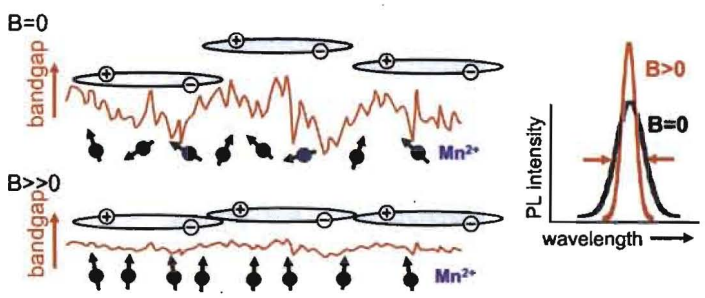

Fig. 4. These drawings illustrate the effects of magnetic field and Mn^{2+} spin orientation on the microscopic alloy (bandgap fluctuation) disorder that is 'seen' by excitons in diluted magnetic semiconductors. As the Mn^{2+} spins align and the potential is smoothed, the PL linewidth is reduced. The presence of Mn-Mn pairs (not depicted here) gives rise to additional, step-wise annealing and – eventually – roughening at high magnetic fields.

Figure 5 shows a simple model of alloy disorder in DMS, using $Zn_{1-x}Mn_xSe$ as an example. Shaded bars represent individual cation sites. Each cation site (either Mn or Zn, with probability x and 1-x) is assigned the local bandgap of its parent compound, giving a fluctuating bandgap as a function of atomic position. Owing to the large J_{sp-d} exchange interaction in DMS,[14] the local bandgap near a Mn cation is strongly dependent on its spin projection, S_z, which can assume values $-\frac{5}{2}, -\frac{3}{2}, ..., +\frac{5}{2}$. Thus, E_{ZnSe}=2.82 eV, and E_{MnSe}=3.4 eV $+\frac{1}{2}(\alpha-\beta)S_z$ eV, where $(\alpha-\beta)$=1.37 eV is the J_{sp-d} exchange integral in $Zn_{1-x}Mn_xSe$.

Statistically, some Mn cations have no magnetic neighbors. These isolated, spin-$\frac{5}{2}$ Mn have Brillouin-like paramagnetic magnetization. In addition, a calculable fraction of Mn cations will have exactly one Mn neighbor. These 'Mn-Mn pairs' bind antiferromagnetically, with total spin S_p=0 at low fields.[14,15] Mn-Mn pairs align in step-wise fashion (giving S_p=1, 2, 3, 4, 5) whenever H equals a multiple of their binding energy, of order 18 T in $Zn_{1-x}Mn_xSe$ and 14 T in $Zn_{1-x}Mn_xTe$.

At H=0 the isolated Mn spins fluctuate, resulting in a large alloy disorder as depicted in Fig. 5(a). Γ can be modeled by the distribution of possible exciton energies, which in turn is computed from the statistics of alloy disorder. An exciton has an energy E given by the average bandgap of the N cation sites within its effective 'volume': $E = N^{-1}\sum_{j=1}^{N} e_j$. The average energy of all excitons, $\langle E\rangle=\mu$, is the mean bandgap and PL line center. The PL linewidth, Γ, is then given by 2.355 times the standard deviation of exciton energies about μ,

$$\langle (E-\mu)^2\rangle^{1/2} = [(P_i\Delta_i^2 - \mu^2)/N]^{1/2}, \quad (1)$$

where P_i is the probability that a particular cation is of type i (*e.g.*, a Zn cation, an isolated Mn with spin S_z, a paired Mn with spin $S_p/2$, etc), Δ_i is the local bandgap of that cation, and a sum over all cation types i is implied.

At low temperatures and in modest fields (H<10 T), all isolated Mn spins align, smoothing the alloy disorder[9,10,11,12] and reducing Γ. However, Mn-Mn pairs

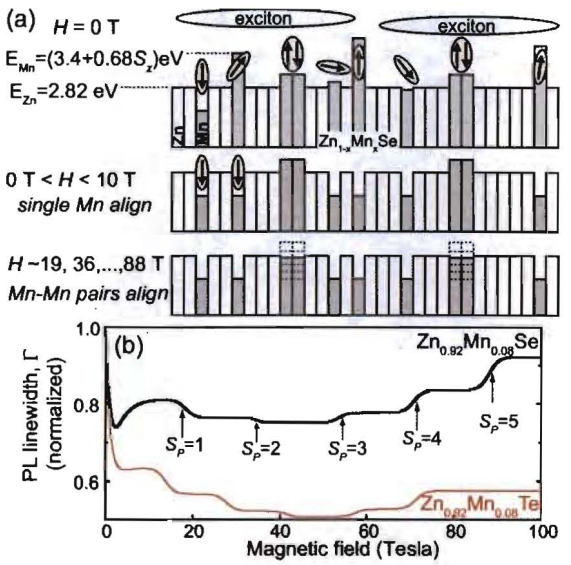

Fig. 5. The drawings represent a simple model of alloy disorder, shown here for the case of $Zn_{1-x}Mn_xSe$. Each cation (Zn or Mn) is assigned the bandgap of its parent compound (see text). At zero field, the isolated $S = \frac{5}{2}$ Mn spins fluctuate, while Mn-Mn pairs have net spin $S_p = 0$. At low fields, the isolated spins align, reducing disorder. At high fields, Mn-Mn pairs align in step-wise fashion, reducing their local bandgap E_p. At the second step at 36 T, E_p falls below the mean bandgap. At subsequent steps (~54, 71, and 88 T), the standard deviation of alloy fluctuations increases again. b) Using this model, this plot shows the PL linewidth calculated for $Zn_{0.92}Mn_{0.08}Se$ and $Zn_{0.92}Mn_{0.08}Te$. Reproduced from Ref (2).

(having S_p=0 and local bandgap E_p=3.4 eV) still present a considerable alloy fluctuation, as drawn. At high H, E_p drops in discrete steps as the pairs align and S_p=1,...,5. In $Zn_{.92}Mn_{.08}Se$, E_p falls just below μ at the second step at ~36 T (as drawn). At this point, the disorder potential is most smooth, and Γ should attain its minimum value. Fig. 5(b) shows Γ calculated for the case of $Zn_{.92}Mn_{.08}Se$. This stepwise "magnetic annealing" has been observed in 60 T fields in $Zn_{1-x-y}Cd_yMn_xSe$ quantum wells.[10]

However, a key prediction of this model is that alloy fluctuations can again *increase* at even larger H in DMS systems (such as $Zn_{1-x}Mn_xSe$ and $Zn_{1-x}Mn_xTe$) where the bandgap of fully-polarized Mn-Mn pairs is less than μ. As Fig. 5 depicts, further alignment of Mn-Mn pairs in $Zn_{.92}Mn_{.08}Se$ at the third, fourth, and fifth magnetization steps reduces E_p to values well below μ, increasing the net alloy disorder – and Γ – once again. These steps occur at ~54, 71, and 88 T, and are therefore observable only in very large magnetic fields.

Fig. 6(a) shows PL spectra at peak field for eight high-field pulses shown in Fig. 2(b). At lower H (0-53 T), over 2000 spectra were acquired in a separate pulse of

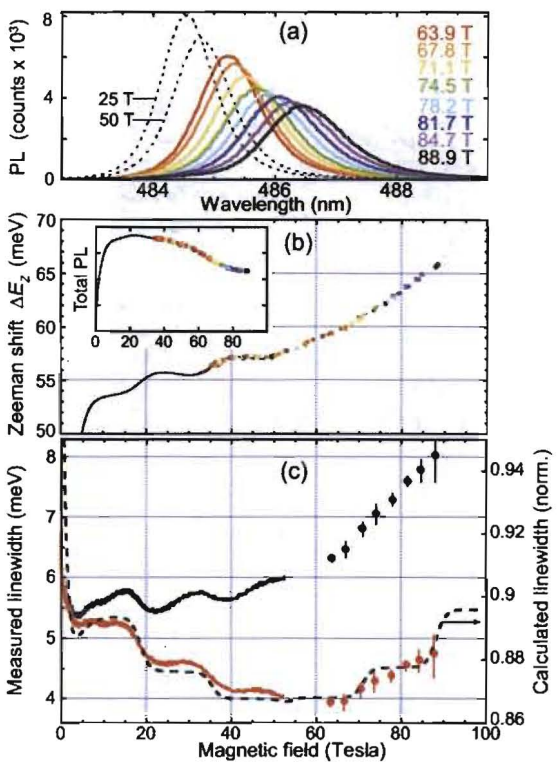

Fig. 6. a) PL spectra acquired at 1.5 K from a $Zn_{0.70}Cd_{0.22}Mn_{0.08}Se$ single quantum well at the magnetic fields indicated. b) The high-field Zeeman energy shift of the PL. The colored points were from data taken in the 100 T magnet, while the black line was from data taken in the 60 T Long Pulse magnet. The inset shows the total integrated PL signal from this quantum well versus applied field. c) The measured Pl linewidth Γ (black). Subtraction of a linearly-increasing background due to field-induced shrinkage of the exciton gives the red data, which agrees well with the expectation from the model (dashed line). Reproduced from Ref. (2).

a 60 T 'Long-Pulse' magnet.[10,17] The spectra have nearly gaussian lineshape, and exhibit a strong Zeeman redshift, ΔE_Z, with increasing H. $\Delta E_Z(H)$ tracks the average bandgap of the quantum well, providing a relative measure of the net Mn magnetization.[14] $\Delta E_Z(H)$ is shown in Fig. 6(b), using data from all high-field pulses (colored points) as well as 0-53 T data (black line). Following the rapid polarization of isolated Mn spins at low H, clear steps at ~19, 36, and 53 T correspond to the first three magnetization steps of Mn-Mn pairs, as observed previously in this and related samples.[10,17] The fourth and fifth steps at ~71 and 88 T are less clear; ΔE_Z increases more smoothly in this regime. The inset shows the total PL intensity.

Figure 6(c) shows the measured PL linewidth, Γ. Raw data is shown in black.

The points are derived from gaussian fits to the peak-field spectra of Fig. 6(a), and the solid line is derived from fitting all the low-field spectra (<53 T). The raw data includes a contribution to Γ that increases nearly linearly with H. This well-known phenomenon results *only* from the field-induced shrinking of an exciton's 'volume'.[8] Smaller excitons are more sensitive to microscopic alloy fluctuations, giving a larger distribution of exciton energies and larger Γ. A linear contribution to Γ is therefore subtracted off, giving the data shown in red. Γ falls quickly at low H (<5 T) as isolated Mn spins align and alloy fluctuations are smoothed. Γ then remains nearly constant until the first magnetization step of Mn-Mn pairs at ~19 T. At this step the net alloy disorder is reduced once again by the partial alignment of Mn-Mn pairs, where the local bandgap E_p drops from 3.4 eV to a value closer to the mean bandgap μ. This 'linewidth annealing' process repeats at the second and third steps. However, the high-field data show that this trend *reverses* at the fourth magnetization step: above 70 T, Γ unambiguously increases. The error bars arise because H is not perfectly constant during the 1.2 ms PL acquisition window near peak field. If $H=H_0 \pm \delta H$ during a PL acquisition, the resulting Zeeman shift, $\partial E_Z/\partial H|_{H_0} \delta H$, acts to increase Γ. In this work, δH=0.8-2.4 T. For the low-field data, δH<0.15 T and errors in Γ are negligible.

The dotted line in Fig. 6(c) shows Γ calculated (and normalized) for $Zn_{.70}Cd_{.22}Mn_{.08}Se$. Γ should reach a minimum at the third step at 54 T, and increase thereafter. This behavior differs slightly from that predicted for $Zn_{.92}Mn_{.08}Se$ in Fig. 5(b). The average bandgap μ in $Zn_{.70}Cd_{.22}Mn_{.08}Se$ is smaller, such that E_p falls just below μ at the third (rather than second) magnetization step. Thus, alloy disorder is not predicted to increase appreciably until the fourth step at 71 T, in clear agreement with the data.

These data therefore confirm a key high-field prediction of 'local-bandgap' models of microscopic alloy fluctuations in DMS. However, although the measured stepwise decrease and subsequent increase of Γ is qualitatively reproduced by the model, the overall magnitude of the effect is not. The measured changes in Γ are larger than calculated: as seen in Fig. 6(c), the calculated linewidth is both scaled and offset. A quantitative discrepancy is not, however, unexpected – as formulated in Eq. 1, this model accounts only for alloy disorder as probed by excitons of *fixed size*. In particular, the model does not attempt to account for any additional effects of exciton localization by alloy disorder. Excitons can delocalize (increasing the number of cations within their volume, N) whenever disorder is smoothed, further reducing Γ at these points. Klar *et al.*[11] have argued that delocalization of this sort must occur in DMS, based on $\Gamma(H)$ studies in $Zn_{.75}Cd_{.16}Mn_{.09}Se$. We therefore suggest that a more complete theory may also account for the degree of delocalization that occurs when Mn spins align at low fields and at each magnetization step.[18] As an indirect measure of localization by disorder, note that the integrated PL (inset, Fig. 6b) roughly tracks the inverse of $\Gamma(H)$, suggesting that non-radiative recombination is suppressed when excitons delocalize in a smoother alloy potential.

Acknowledgements

We gratefully acknowledge J. Sims and the magnet design group, and the 100 T commissioning team: C. Swenson, E. Serna, J. Schillig, P. Ruminer, D. Roybal, D. Rickel, A. Paris, M. Pacheco, J. Michel, J. Martin, M. Gordon, and J. Betts. This work was directly supported by the National Science Foundation, the U.S. Department of Energy, and the State of Florida.

1. G. Boebinger, Physics Today **49**, 36 (1996).
2. S. A. Crooker and N. Samarth, Appl. Phys. Lett. **90**, 102109 (2007).
3. N. Harrison *et al.*, Phys. Rev. Lett. **99**, 056401 (2007).
4. E. Yelland *et al.*, Phys. Rev. Lett. **100**, 047003 (2008).
5. D. Andronikov*et al.*, Phys. Rev. B **72**, 165339 (2005); G. V. Astakhov *et al.*, Phys. Rev. B **71**, 201312(R) (2005).
6. O. Goede, L. John, D. Hennig, Phys. Stat. Sol. B **89**, K183 (1978).
7. E. F. Schubert *et al.*, Phys. Rev. B **30**, 813 (1984); J. Singh, K. K. Bajaj, Appl. Phys. Lett. **44**, 1075 (1984).
8. R. A. Mena *et al.*, J. Appl. Phys. **70**, 1866 (1991); E. D. Jones, R. P. Schneider, S. M. Lee, K. K. Bajaj, Phys. Rev. B **46**, 7225 (1992); S. K. Lyo, Phys. Rev. B **48**, 2152 (1993).
9. S. M. Ryabchenko, Y. G. Semenov, O. V. Terletskii, Sov. Phys. Solid State **27**, 1746 (1985).
10. S. A. Crooker, D. G. Rickel, S. K. Lyo, N. Samarth, D. D. Awschalom, Phys. Rev. B **60**, R2173 (1999).
11. P. J. Klar, H. Falk, W. Heimbrodt, Solid State Comm. **116**, 125 (2000).
12. A. V. Komarov *et al.*, J. Phys. Cond. Mat. **18**, 7401 (2006).
13. J. Sims *et al.*, IEEE Trans. Appl. Supercon. **10**, 510 (2000).
14. J. K. Furdyna, J. Appl. Phys. **64**, R29 (1988).
15. Y. Shapira and V. Bindilatti, J. Appl. Phys. **92**, 4155 (2002); Y. Shapira *et al.*, Phys. Rev. B **30**, 4021 (1984); S. Foner *et al.*, Phys. Rev. B **39**, 11793 (1989).
16. S. A. Crooker *et al.*, Phys. Rev. Lett. **75**, 505 (1995).
17. S. A. Crooker, N. Samarth, D. D. Awschalom, Phys. Rev. B **61**, 1736 (2000).
18. M. E. Raikh and Al. L Efros, Sov. Phys. Solid State **26**, 61 (1984).